Supplementary Information

A high-performance Iron–Tetrahydroxyanthraquinone Metal–Quinone network for Solid-State Organic Batteries

Kaiwen Li,[a] Yanpeng Fan,[a] Yu Shi,[a] Runya Han,[a] Ping He,[a] and Haoshen Zhou*[a]

[a] Center of Energy Storage Materials & Technology, College of Engineering and Applied Sciences, Jiangsu Key Laboratory of Artificial Functional Materials, National Laboratory of Solid-State Microstructures and Collaborative Innovation Center of Advanced Microstructures, Nanjing University, Nanjing 210093, China.

*Corresponding authors. E-mail: hszhou@nju.edu.cn

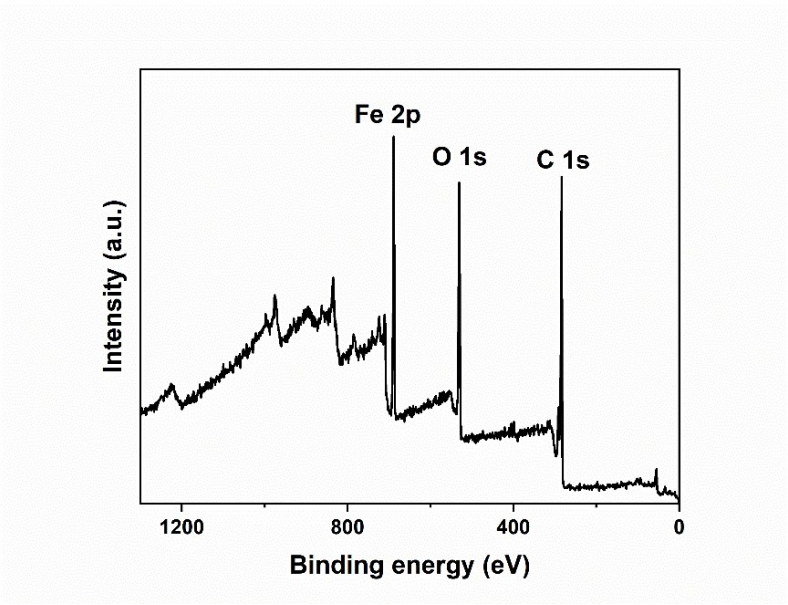

Fig. S1. XPS survey spectrum of Fe-THAQ.

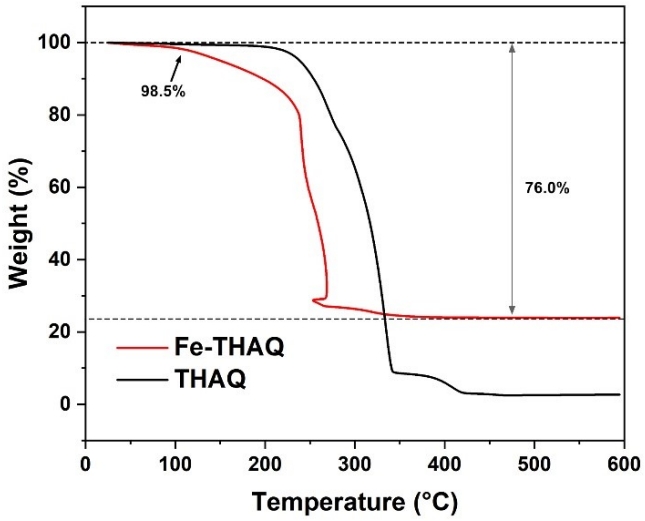

Fig. S2. TG curves of THAQ and Fe-THAQ under air atmosphere.

The content of Fe (ω_{Fe}) in the Fe-THAQ sample could be calculated by the following equation,

$$\omega_{Fe} = 24.0\% \div 98.5\% \times 69.9\% = 17.0\%$$

where 24.0%was the remained weight percentage after 600 ^{o}C, 98.5% was the weight percentage of Fe-THAQ in the sample, and 69.9% is the mass fraction of Fe in Fe_2O_3.

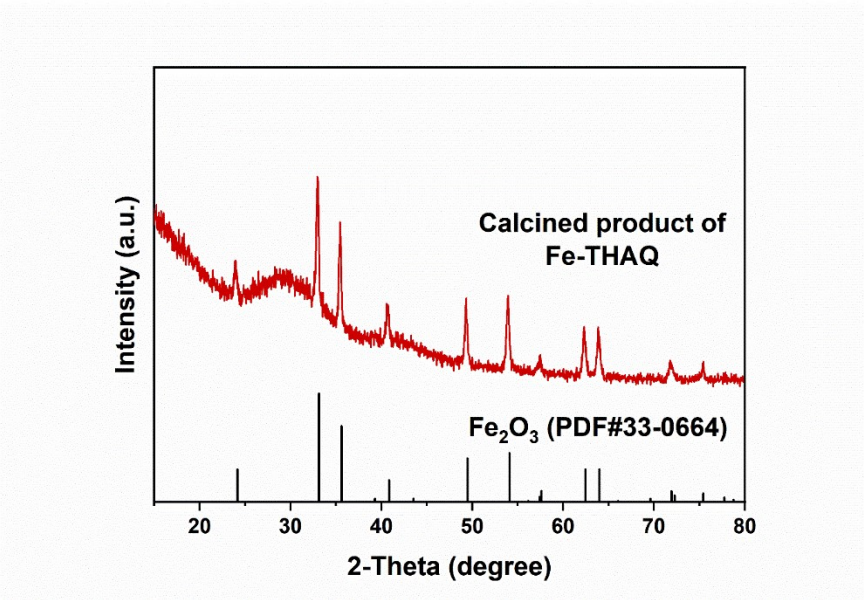

Fig. S3. XRD pattern of the calcined product of Fe-THAQ after heating to 600 °C in air atmosphere, and the standard Fe_2O_3 (PDF# 33-0664).

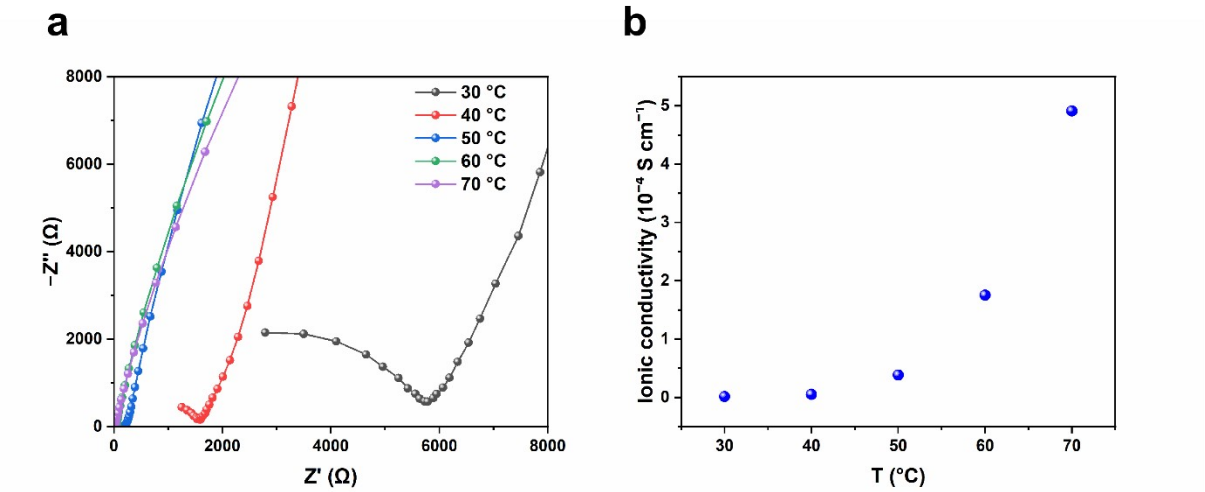

Fig. S4 (a) The Nyquist plot of the LiTFSI/PEO solid-state electrolyte film and (b) the corresponding ionic conductivity at different temperatures.

The ionic conductivity was calculated by the following formula:

$$\sigma = L/(R_b \times S)$$

At 70 °C, L is the membrane thickness (0.0156 cm), R_b is 15.8 Ω (obtained from the intercept of the curve with Z'-axis), and S is the electrode area (2.01 cm^2). The calculated ionic conductivity at was 4.91×10^{-4} S cm^{-1}. Similarly, the ionic conductivities of PEO at 30, 40, 50, 60 °C were 1.34×10^{-6}, 4.88×10^{-6}, 3.82×10^{-5}, 1.75×10^{-4} S cm^{-1}, respectively.

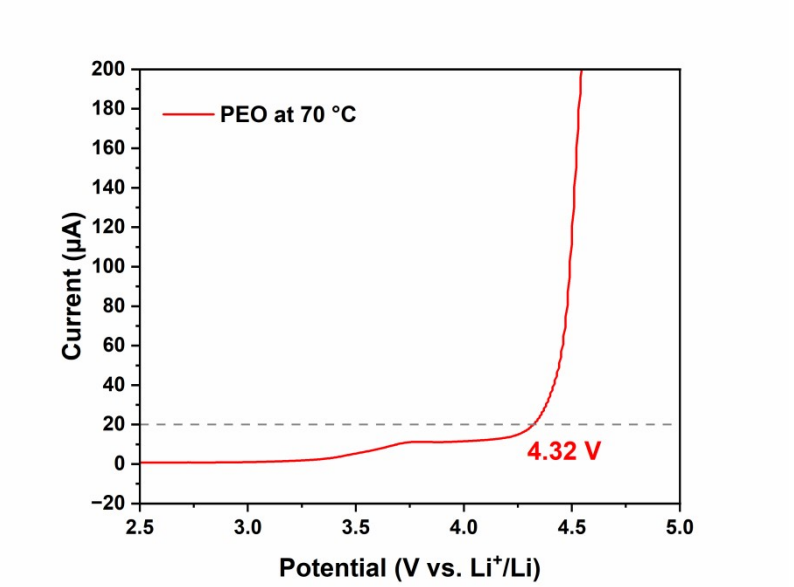

Fig. S5 LSV of the LiTFSI/PEO solid state electrolyte at 70 °C. Test was performed in a two-electrode configuration using lithium foil as the counter/reference electrode and an Al-carbon composite as the working electrode, with a scan rate of 1 mV s^{-1} over a voltage range of 2.1–5.5 V.

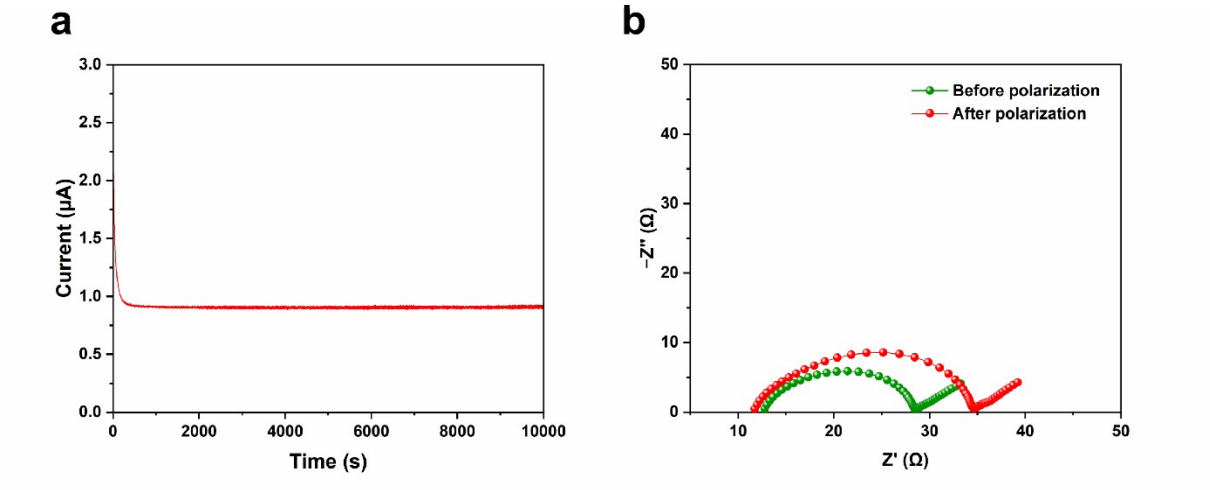

Fig. S6 (a) DC polarization and (b) Nyquist plots of the Li||PEO||Li cell before and after polarization at 70 °C.

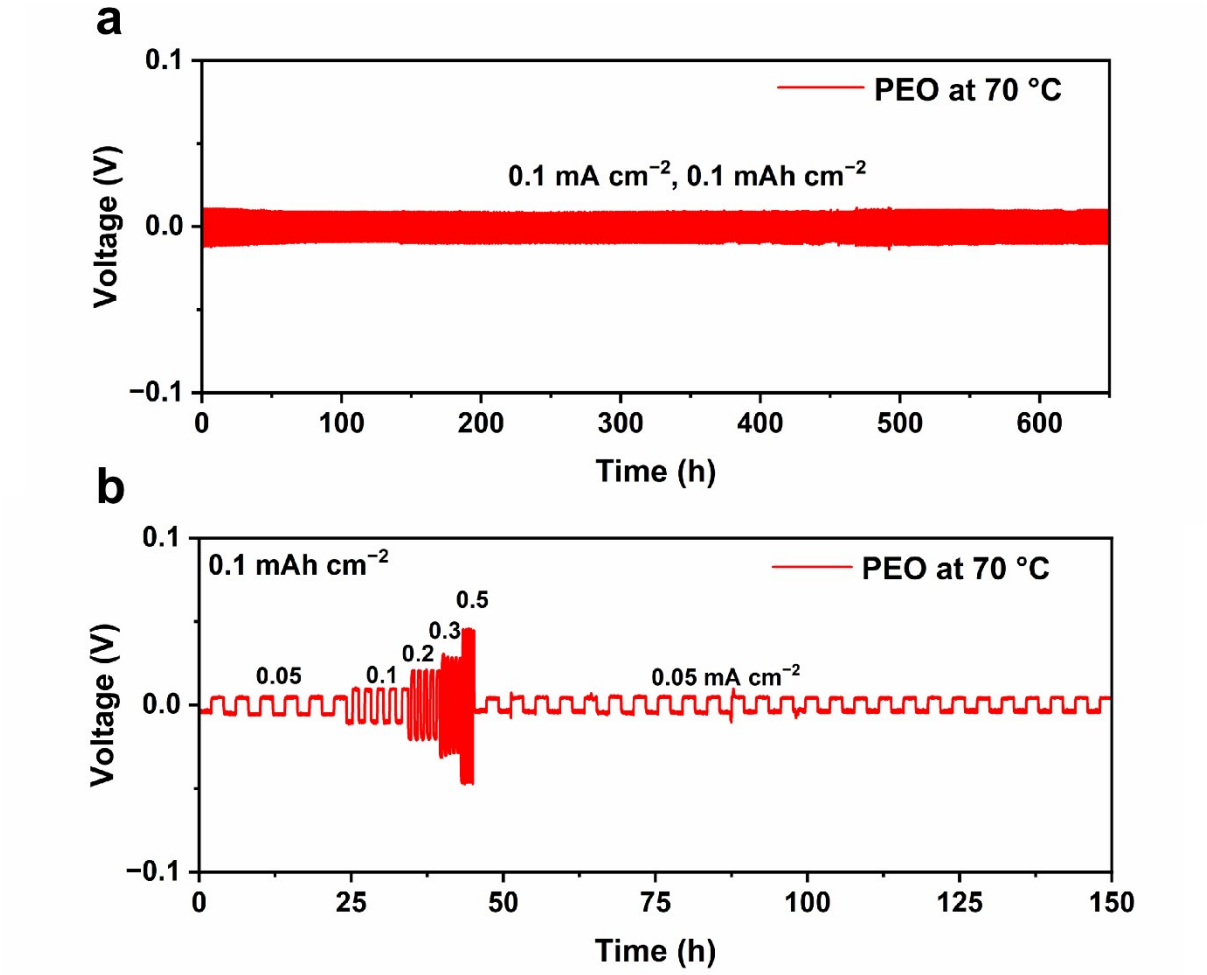

Fig. S7 Voltage-time profiles of symmetric Li metal batteries in PEO electrolyte at (a) 0.1 mA cm^{-2}, 0.1 mAh cm^{-2} and (b) different current densities.

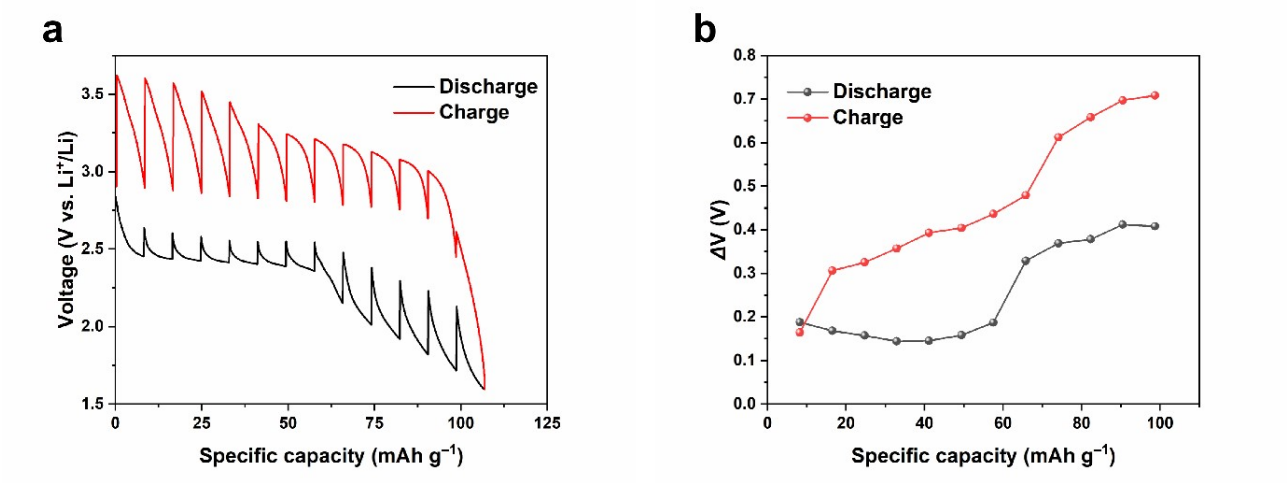

Fig. S8 (a) GITT potential profile and (b) the corresponding polarization plots of THAQ during the first discharge/charge cycle.

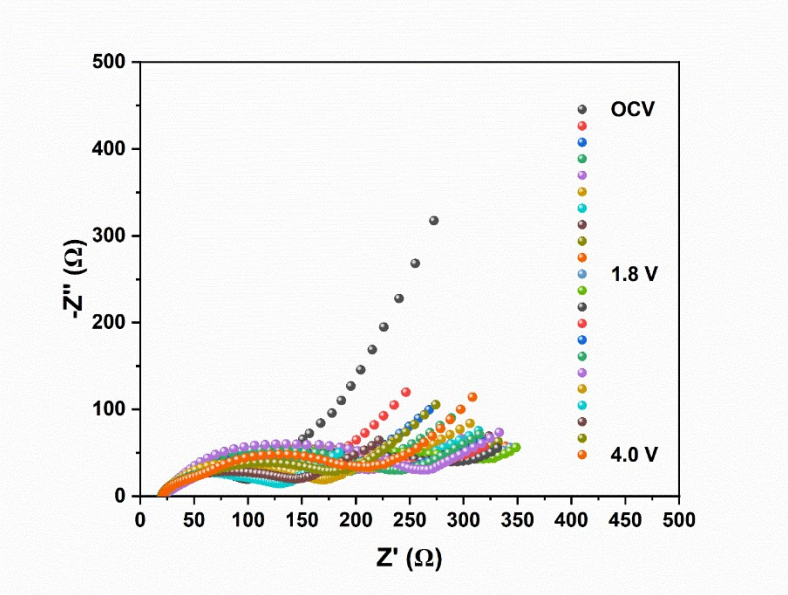

Fig. S9 In-situ EIS data (Nyquist plots) during the first cycle of the Fe-THAQ/PEO/Li cell.

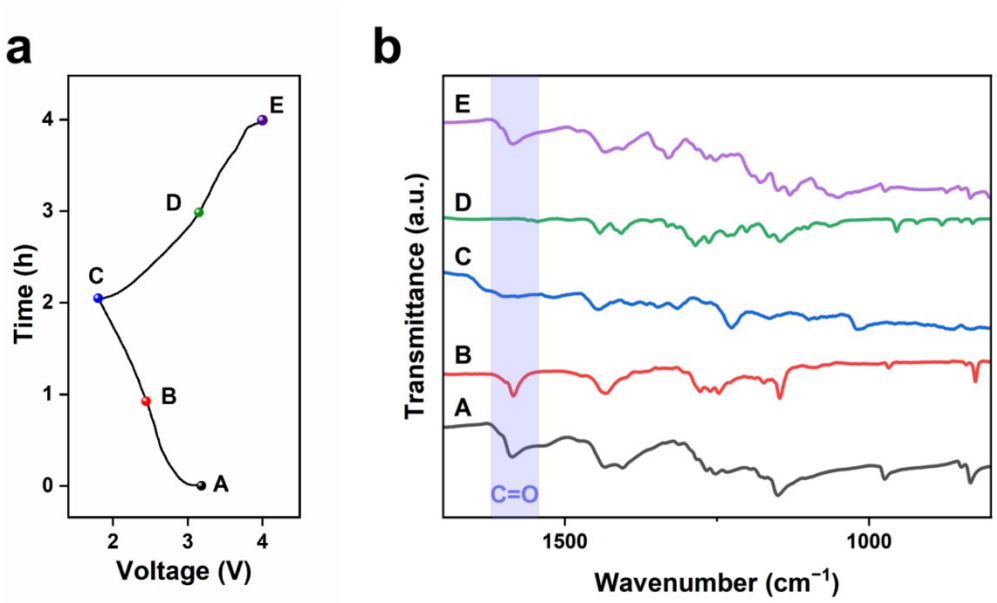

Fig. S10 Ex situ infrared spectra of Fe-THAQ. (a) voltage profiles presenting the sampling points and (b) the corresponding IR spectra.

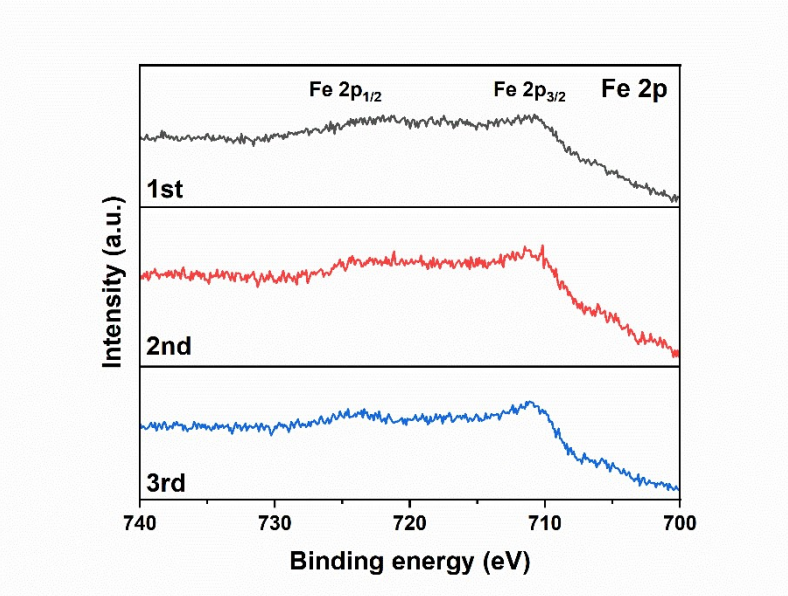

Fig. S11 Fe 2p XPS spectra of the Fe-THAQ electrode after the first, second, and third cycles.

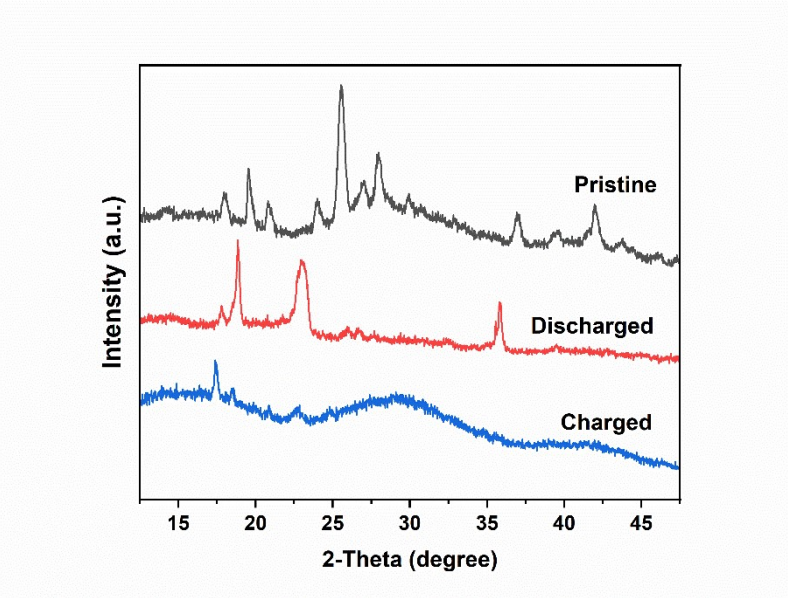

Fig. S12 XRD patterns of Fe-THAQ in different states of the initial cycle.

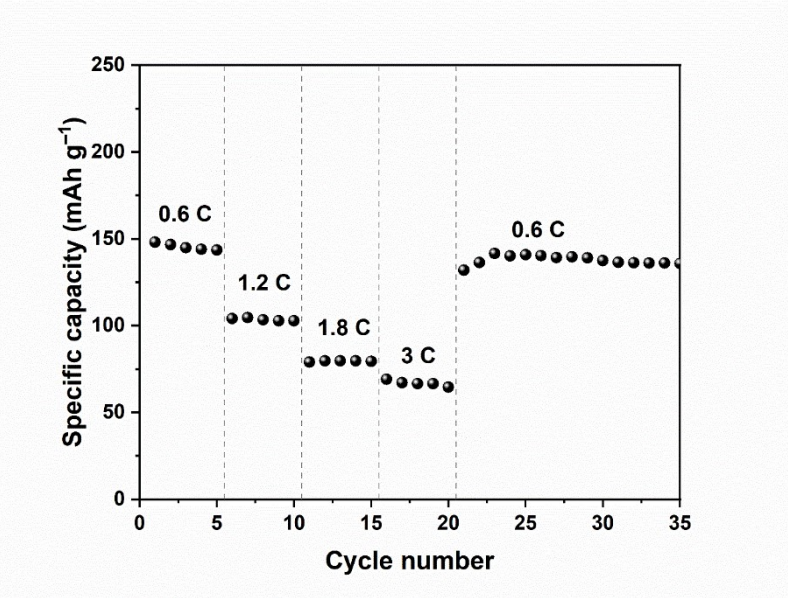

Fig. S13 Capacity related to C-rates.

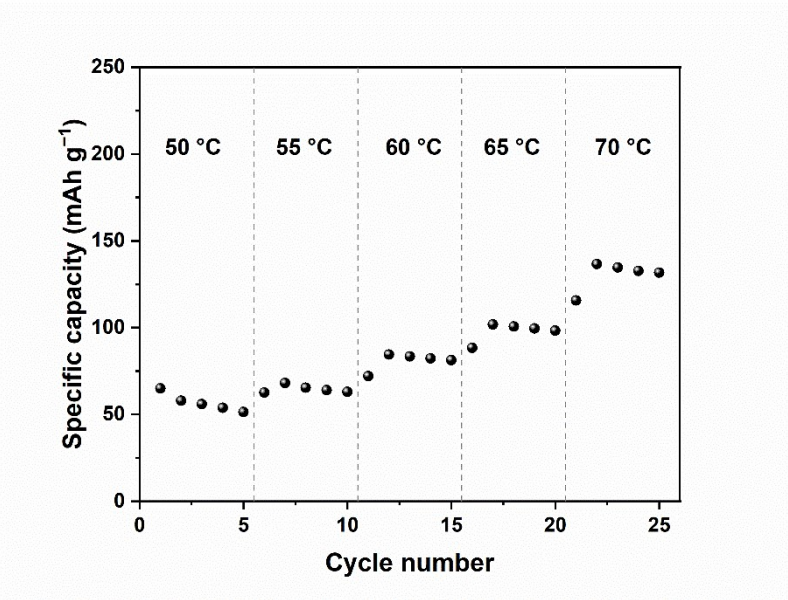

Fig. S14 Cycling performance of Fe-THAQ||PEO||Li cells at 50 to 70 °C.

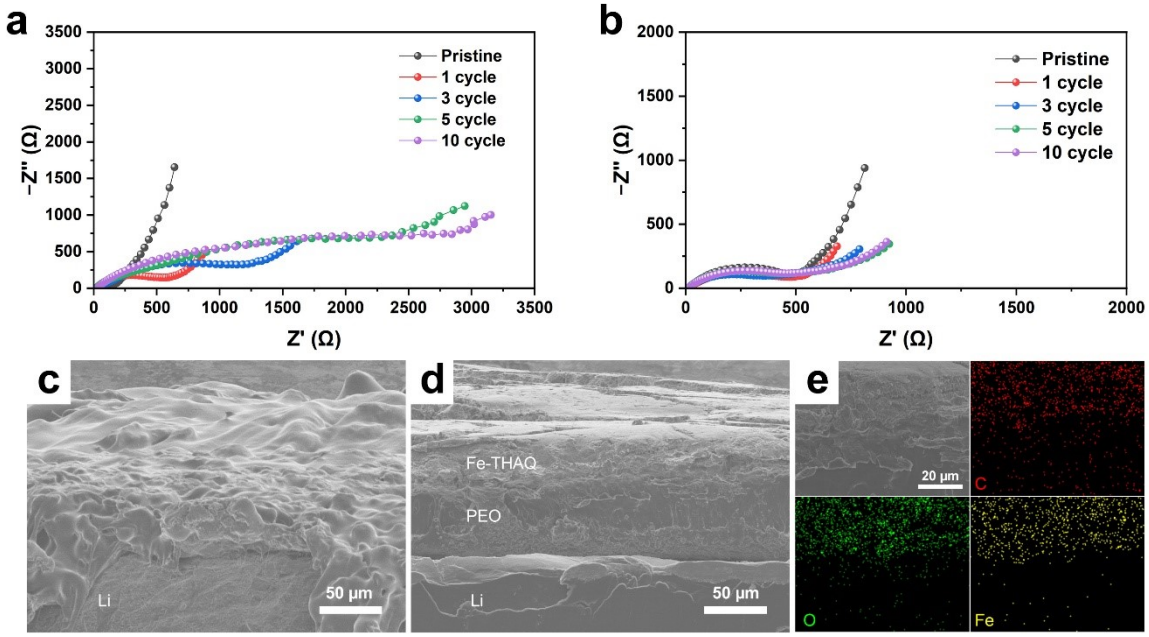

Fig. S15 The Nyquist plot of (a) THAQ||PEO||Li and (b) Fe-THAQ||PEO||Li cells after different numbers of cycles. Cross-sectional SEM images of (c) THAQ||PEO and (d) Fe-THAQ||PEO after 10 cycles. (e) SEM-EDS mapping of Fe, O, and C elements in the Fe-THAQ||PEO interface after 10 cycles.

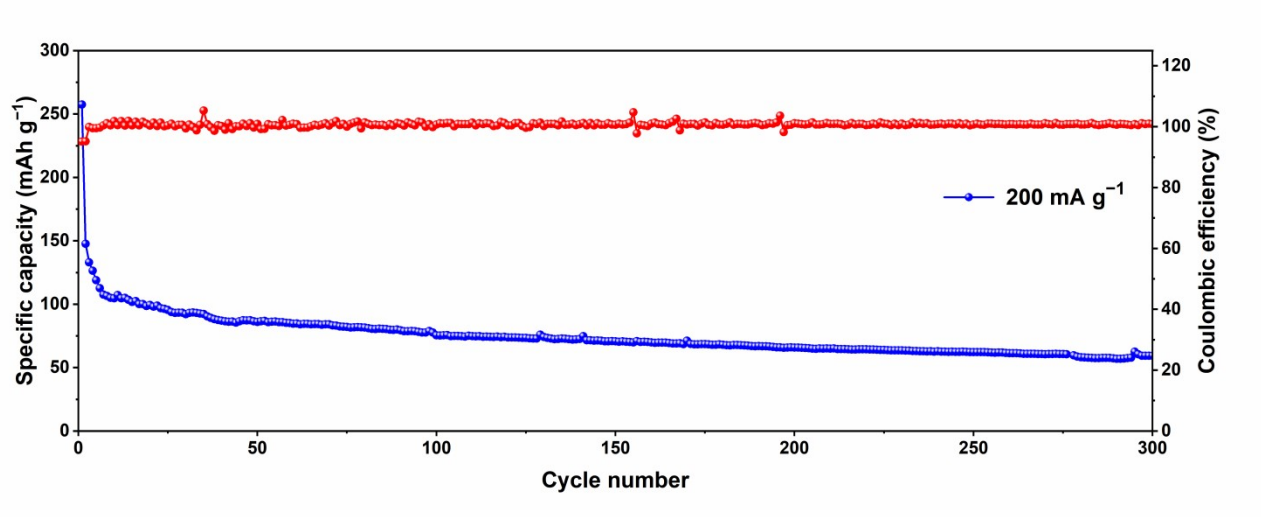

Fig. S16 Long-term cycling performance of Fe-THAQ||PEO||Li cells at 200 mA g^{-1} at 70 °C.

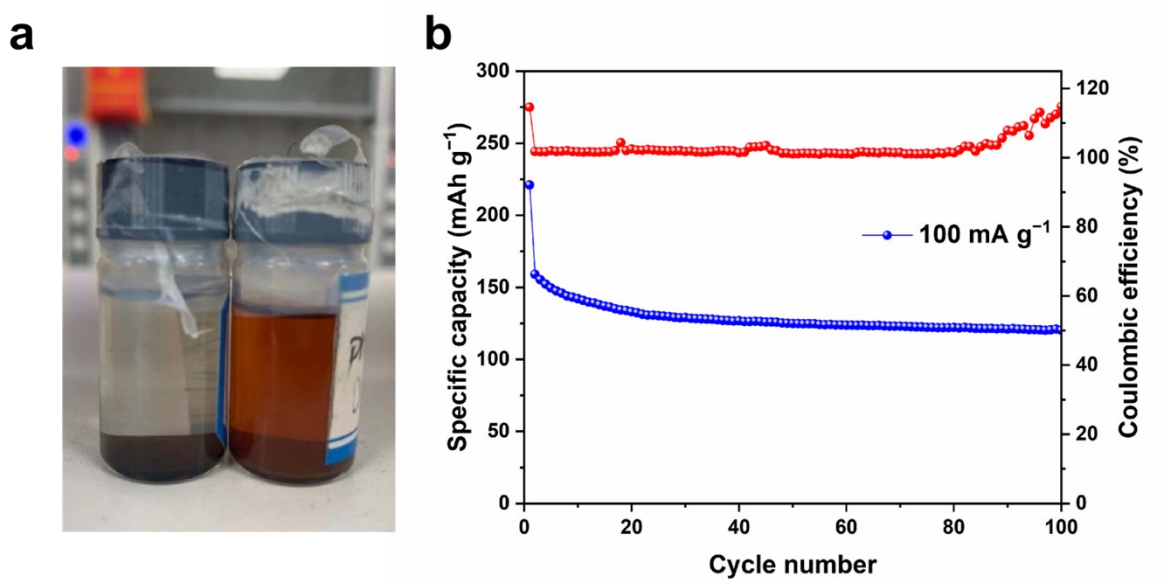

Fig. S17 (a) Digital photo of Fe-THAQ and THAQ after immersion in electrolyte (1M LiTFSI in DOL/DME, v% = 1:1) for 24 h. (b) long-term cycling performance of Fe-THAQ with liquid electrolyte (1M LiTFSI in DOL/DME, v% = 1:1) at 100 mA g^{-1} within 1.8–3.6 V.

Table S1. Properties of PEO at 70 °C.

Ionic conductivity	Electrochemical window	Li^+ transference number	overpotential
4.91×10^{-4} S cm^{-1}	4.32 V	0.29	5 mV (0.05 mA cm^{-2}) 11 mV (0.1 mA cm^{-2}) 20 mV (0.2 mA cm^{-2}) 29 mV (0.3 mA cm^{-2}) 45 mV (0.5 mA cm^{-2})

Table S2. The physical processes corresponding to the fitted relaxation times from the DRT analysis.

Time Constant	Approximate Range (s)	Corresponding process
τ_1	10^{-4}–10^{-3}	Li^+ transport through the SEI layer at Li/SSE interface
τ_2	10^{-3}–10^{-2}	Resistance at active material of cathode/SSE interface
τ_3	10^{-2}–10^{0}	Charge-transfer process at Li/SSE or cathode/SSE interfaces

Table S3. Cycling performance comparison of reported researches on lithium-organic batteries under corresponding test conditions.

Cathode	Electrode	Reversible capacity (mAh g^{-1})	Current	cycles	Ref.
Fe-THAQ	**PEO**	**150**	**100 mA g^{-1}**	**300**	**This work**
PQ	LZC	~150	0.3 C	100	S1
PI	LPSC	~160	0.1 C	300	S2
F_4TCNQ	PEO-LLZTO	~150	10 mA g^{-1}	50	S3
PCS	LiTFSI-DME/DOL	~130	4 C	200	S4
TTF-Ph-COF	$LiPF_6$-EC/DMC	~55	2 C	400	S5
NR	-	125	50 mA g^{-1}	200	S6
P-NDI	LiTFSI-DME/DOL	~120	50 mA g^{-1}	400	S7

References

S1 Gao, Y.; Fu, J.; Hu, Y.; Zhao, F.; Li, W.; Deng, S.; Sun, Y.; Hao, X.; Ma, J.; Lin, X.; Wang, C.; Li, R.; Sun, X. Reviving Cost-Effective Organic Cathodes in Halide-Based All-Solid-State Lithium Batteries. *Angew. Chem. Int. Ed.* 2024, ***63***, e202403331.

S2 Ji, W.; Zhang, X.; Qu, H.; Xin, L.; Luedtke, A. T.; Huang, H.; Lambert, T. H.; Qu, D. Polyimide as a Durable Cathode for All-Solid-State Li(Na)−organic Batteries with Boosted Cell-Level Energy Density. *Nano Energy* 2022, ***96***, 107130.

S3 Geng, Z.; Shi, W.; Wang, J.; Zhang, X.; Hu, N.; Wang, S.; Deng, W. A High-Voltage Solid-State Organic Lithium Battery Based on 2,3,5,6-Tetrafluoro-7,7,8,8-Tetracyanoquinodimethane Cathode. *Int. J. Energy Res.* 2022, ***46***, 12316–12322.

S4 Goujon, N.; Cubero-Cardoso, J.; Urbano, J.; Mecerreyes, D. Bioinspired Poly(Catechol Sulfide) as Organic Cathode Materials for Lithium Metal Batteries. *J. Mater. Chem. A* 2025, **13**, 132528–32538.

S5 Valente, G.; Dantas, R.; Ferreira, P.; Grieco, R.; Patil, N.; Guillem-Navajas, A.; Rodríguez-San Miguel, D.; Zamora, F.; Guntermann, R.; Bein, T.; Rocha, J.; Braga, M. H.; Strutyński, K.; Melle-Franco, M.; Marcilla, R.; Souto, M. Tetrathiafulvalene-Based Covalent Organic Frameworks as High-Voltage Organic Cathodes for Lithium Batteries. *J. Mater. Chem. A* 2024, ***12***, 24156–24164.

S6 Liao, D.; Yang, Y.; Jia, J.; Liu, Z.; Fan, L.; Xin, J. H.; Han, S.; Liu, X. A Nile Red Dye Cathode with an Asymmetric Redox Unit for Lithium Organic Batteries. *Chem. Commun.* 2024, ***60***, 11762–11765.

S7 Zhang, B.; Zhang, Y.; Yang, X.; Li, G.; Zhang, S.; Zhang, Y.; Yu, D.; Liu, Z.; He, G. Isometric Thionated Naphthalene Diimides as Organic Cathodes for High Capacity Lithium Batteries. *Chem. Mater.* 2020, ***32***, 10575–10583.